Biophysical Journal
Article

Biophysical Society

Membrane Potential Distinctly Modulates Mobility and Signaling of IL-2 and IL-15 Receptors in T Cells

Éva Nagy,[1] Gábor Mocsár,[1] Veronika Sebestyén,[1] Julianna Volkó,[1] Ferenc Papp,[1,2] Katalin Tóth,[3] Sándor Damjanovich,[1] György Panyi,[1,2] Thomas A. Waldmann,[4] Andrea Bodnár,[1] and György Vámosi[1,*]

[1]Department of Biophysics and Cell Biology, Faculty of Medicine; [2]MTA-DE- NAP B Ion Channel Structure-Function Research Group, RCMM, University of Debrecen, Debrecen, Hungary; [3]Division Biophysics of Macromolecules, German Cancer Research Center, Heidelberg, Germany; and [4]Lymphoid Malignancies Branch, National Institutes of Health, Bethesda, Maryland

ABSTRACT The high electric field across the plasma membrane might influence the conformation and behavior of transmembrane proteins that have uneven charge distributions in or near their transmembrane regions. Membrane depolarization of T cells occurs in the tumor microenvironment and in inflamed tissues because of K^+ release from necrotic cells and hypoxia affecting the expression of K^+ channels. However, little attention has been given to the effect of membrane potential (MP) changes on membrane receptor function. Therefore, we studied the influence of membrane de- and hyperpolarization on the biophysical properties and signaling of interleukin-2 (IL-2) and interleukin-15 (IL-15) receptors, which play important roles in T cell function. We investigated the mobility, clustering, and signaling of these receptors and major histocompatibility complex (MHC) I/II glycoproteins forming coclusters in lipid rafts of T cells. Depolarization by high K^+ buffer or K^+ channel blockers resulted in a decrease in the mobility of IL-2Rα and MHC glycoproteins, as shown by fluorescence correlation spectroscopy, whereas hyperpolarization by the K^+ ionophore valinomycin increased their mobility. Contrary to this, the mobility of IL-15Rα decreased upon both de- and hyperpolarization. These changes in protein mobility are not due to an alteration of membrane fluidity, as evidenced by fluorescence anisotropy measurements. Förster resonance energy transfer measurements showed that most homo- or heteroassociations of IL-2R, IL-15R, and MHC I did not change considerably, either. MP changes modulated signaling by the two cytokines in distinct ways: depolarization caused a significant increase in the IL-2-induced phosphorylation of signal transducer and activator of transcription 5, whereas hyperpolarization evoked a decrease only in the IL-15-induced signal. Our data imply that the MP may be an important modulator of interleukin receptor signaling and dynamics. Enhanced IL-2 signaling in depolarized T_{reg} cells highly expressing IL-2R may contribute to suppression of antitumor immune surveillance.

INTRODUCTION

Interleukin-2 receptors (IL-2R) and interleukin-15 receptors (IL-15R) and class I and II MHC glycoproteins have essential roles in immune responses. IL-2 and IL-15 are important regulators of T cell proliferation, activation, survival, and cell death (1,2). Both IL-2 and -15 receptors consist of three subunits: the ligand-specific α-chains (IL-2Rα and IL-15Rα) and the β- and γ_c-chains, which are shared by the two cytokines and are responsible for signal transduction. The binding of cytokines to these receptors activates the Janus-faced kinase/signal transducer and activator of transcription (Jak/STAT), mitogen-activated protein kinase, and phosphatidylinositol-3-kinase pathways, resulting in a set of similar effects, including the stimulation of T- and NK cell proliferation. However, they also have antagonistic effects: IL-2 promotes activation-induced cell death, an apoptotic process resulting in downregulation of the immune response and contributing to peripheral self-tolerance, whereas IL-15 inhibits apoptosis and facilitates long-term survival of memory T cells (3). It remains to be clarified how the two cytokines can lead to divergent cell fates despite sharing the signaling receptor subunits. MHC I (present on all nucleated cells) and MHC II glycoproteins (expressed by professional antigen-presenting cells and several activated and tumor cells) present antigen peptides to T cell receptors, thereby inducing T cell activation (4). MHC I consists of a transmembrane heavy chain and the extracellular β2-microglobulin (β2m) lacking a transmembrane region, whereas MHC II has two transmembrane subunits. According to our previous investigations, IL-2R, IL-15R, and MHC I and II are all coexpressed in lipid rafts of T lymphoma cells forming homo- and heteroaggregates that diffuse stably together (5–9).

Submitted March 7, 2018, and accepted for publication April 23, 2018.

*Correspondence: vamosig@med.unideb.hu

Éva Nagy and Gábor Mocsár contributed equally to this work.

Editor: Anne Kenworthy.

https://doi.org/10.1016/j.bpj.2018.04.038

The assembly, mobility, and function of membrane receptors may be modulated by multiple environmental factors, such as the lipid environment, interactions with other membrane proteins, or the cytoskeleton. Cholesterol depletion reduced the activity of IL-2R and delayed signaling by IL-9R in human $CD4^+$ T lymphoma cells (6,10), whereas cholesterol enrichment enhanced the basal level of signal transducer and activator of transcription 5 (STAT5) phosphorylation in mouse $CD4^+$ T cells (11). Knocking down MHC I coclustered with IL-2/15R increased the mobility of both receptor types (7). Binding of IL-2 enhanced the attachment of IL-2R to the cytoskeleton, thereby reducing its mobility (12). IL-4 signaling can be blocked by inhibiting actin polymerization driving receptor internalization (13). The properties of transmembrane proteins having an uneven charge distribution may be affected by an electric field. However, little attention has been given to the influence of the membrane potential (MP) on the biophysical properties and function of membrane receptors.

During their development and functional activity, T lymphocytes are often exposed to changes of MP in various milieus. In the tumor microenvironment, rapid cell division and competition for limited local resources can produce necrotic or apoptotic areas, where dying cells release their intracellular ions to the extracellular space. In turn, the increase of extracellular K^+ concentration, $[K^+]_e$, depolarizes T cells expressing K^+ channels such as Kv1.3, the dominant voltage gated K^+ channel on T cells (14). Necrosis, and a similar increase of $[K^+]_e$, may also occur in inflamed tissues. Depolarization can also take place as a result of the altered expression of ion channels. Hypoxic conditions may disrupt forward vesicular trafficking of Kv1.3 and reduce its cell surface expression in T cells, leading to membrane depolarization (15). Hypoxic areas have been detected, e.g., in lymph nodes and spleen, wounds, solid tumors, and joints with rheumatoid arthritis (16–19).

Transmembrane proteins usually contain positively charged amino acids in the cytoplasmic flanks of the transmembrane regions (TMRs) (positive-inside rule (20)), as necessitated by the electrostatic potential of the cell membrane. Recent statistics derived from a large body of protein sequences demonstrated that negatively charged residues preferentially occur at the extracellular flank of the TMR, or at least they are suppressed at the cytoplasmic flank (negative-not-inside/negative-outside rule (21)). These charges are important determinants of transmembrane protein topology. IL-2/15R subunits also contain charged amino acids near their TMRs. In addition, the β- and γ_c-chains become phosphorylated by Janus-faced kinases (Jak1 and Jak3) upon ligand binding, which adds negative charges of their intracellular tails. It is plausible to assume that the electric field in or near the plasma membrane might influence the biophysical properties and functional activity of these receptors. In our experiments, we investigated the effect of membrane de- and hyperpolarization on the mobility, interactions, and signaling efficiency of these receptors and of MHC I and II glycoproteins coclustered with them. We found significant and distinct changes in the mobility of almost all the above proteins upon de- and hyperpolarization. The signaling efficiency by IL-2 or IL-15 was also affected in distinct ways for the two cytokines. On the other hand, we found no evidence for any large-scale rearrangements in the homo- and heteroclustering patterns of these proteins.

To explore the scope of validity of our findings regarding receptor mobility, we also studied other raft- or non-raft-localized molecules as controls. CD48 is an extracellular glycophosphatidylinositol (GPI)-anchored protein connected to the cell membrane with saturated fatty acid chains, leading to their enrichment in rafts (22). $DiIC_{18}(3)$ is a lipophilic membrane stain also having long saturated fatty acid chains leading to its enrichment in liquid-ordered domains related to rafts (23). Transferrin receptor (CD71) is a nonraft transmembrane protein responsible for iron ion transport; this protein is enriched in coated pits (24). The mobility of these molecules was not altered upon changes of the MP. The change of MP may also influence the general properties of the plasma membrane, such as its fluidity. We monitored membrane fluidity by the fluorescence anisotropy of two membrane probes (diphenyl-hexatriene (DPH) and trimethylammonium DPH (TMA-DPH)) and found that this parameter was not influenced by depolarization.

Our data may shed light on a new regulatory mechanism of the MP on receptor function and mobility and may contribute to understanding the different outcomes of IL-2 and IL-15 signaling. The enhancement of IL-2 signaling efficiency upon membrane depolarization in regulatory T cells (T_{reg} cells) may contribute to suppression of the antitumor surveillance function of effector T cells in the tumor microenvironment.

MATERIALS AND METHODS

Cell culture

Kit 225 K6 (25) and Kit 225 FT7.10 human $CD4^+$ chronic lymphocytic leukemia T cell lines were grown in a 5% CO_2 humidified atmosphere in Roswell Park Memorial Institute medium 1640 (Sigma, St. Louis, MO) and supplemented with 10% (v/v) fetal calf serum, penicillin, and streptomycin (all from Gibco, Carlsbad, CA) and 500 pM human recombinant IL-2 (Hoffmann-La Roche, Basel, Switzerland) every 48 h. Both cell lines express the three subunits of IL-2R. FT7.10 cells are K6 cells stably transfected with N-terminally FLAG-tagged IL-15Rα. The medium of FT7.10 cells contained 0.8 mg/mL G418 (Merck, Darmstadt, Germany) to suppress the growth of wt. cells.

Fluorescence labeling of cells

Membrane proteins were labeled with monoclonal antibodies or their Fab fragments conjugated with Alexa488, Alexa546, Alexa647 (Molecular Probes, Eugene, OR), or Cy3 (Amersham Pharmacia, Little Chalfont, UK). The following antibodies were used (Table 1).

TABLE 1 Antibodies Used for Labeling Membrane Proteins

Protein	Antibody
IL-2Rα	anti-Tac (Repligen Corporation, Needham Heights, MA (48))
IL-15Rα	anti-FLAG (Sigma-Aldrich)
MHC I heavy chain	W6/32 (prepared from hybridoma (49))
β2-microglobulin	L368 (prepared from hybridoma (50))
MHC II	L243 (prepared from hybridoma (51))
CD71 (transferrin receptor)	MEM75 (Exbio Praha, Prague, Czech Republic)
CD48 (GPI-anchored protein)	MEM102 (Exbio Praha)

Harvested cells were washed twice in ice-cold Hanks's balanced salt solution (HBSS) incubated with fluorescently labeled Fab fragments or mAbs (monoclonal antibodies) for 30 min on ice (3 and 5 μg/10^6 cells in 50 μL final volume), washed twice, and resuspended in HBSS.

In fluorescence correlation spectroscopy experiments, we used $DiIC_{18}$ (Molecular Probes) as a control, which is a red fluorescent lipophilic molecule with two saturated fatty acid chains, thus staining the cell membrane. Before staining, the $DiIC_{18}$ stock solution was sonicated, airfuged, and filtered through a 0.2 μm polycarbonate filter (Sigma-Aldrich) to exclude aggregates. Cells were washed and resuspended in HBSS, incubated with $DiIC_{18}$ at a concentration of 1.5 μg/mL for 3 min at 37°C, finally washed, and resuspended in HBSS.

De- and hyperpolarizing treatments

Control cells were suspended in HBSS having the following solute concentrations (in mM): 142.3 NaCl, 1 $CaCl_2$, 0.75 $MgSO_4 \times 7\ H_2O$, 0.44 NaH_2PO_4, 0.33 $Na_2HPO_4 \times 12\ H_2O$, 5.55 glucose, and 10 HEPES (pH 7.4). To depolarize the cell membrane in a controlled way, we incubated cells during measurement in a high-K^+ buffer solution (K-HBSS) containing (in mM): 142.3 KCl, 1 $CaCl_2$, 0.75 $MgSO_4 \times 7\ H_2O$, 0.44 KH_2PO_4, 0.33 K_2HPO_4, 5.55 glucose, and 10 HEPES (pH 7.4). Alternatively, we used margatoxin (MgTx; Alomone Labs, Jerusalem, Israel) (26), a Kv1.3 channel blocker (K_d: 30 pM) at a concentration of 1.5 nM for fluorescence experiments and 250 pM for patch clamp experiments. Hyperpolarization was achieved by treatment with 10 μM valinomycin (Sigma-Aldrich), a K^+ ionophore (27). According to the Goldman-Hodgkin-Katz equation (28), when the extracellular K^+ concentration is high or the permeability of the membrane to potassium ions is low (channels are blocked), the resting MP is shifted in the positive direction. Upon permeabilizing the membrane to K^+ ions by valinomycin, the resting MP is shifted in the negative direction. We tested the efficiency of our depolarizing and hyperpolarizing methods by patch clamp. Fluorescence measurements were started after ~10 min incubation in the de- or hyperpolarizing solutions. The duration of live cell measurements did not exceed 30 min to preserve cell viability.

Electrophysiology

The patch-clamp technique in current-clamp mode was used to measure the MP (Multiclamp 700B amplifier; Molecular Devices, San Jose, CA). The bath solution was (in mM) as follows: 145 NaCl, 5 KCl, 1 $MgCl_2$, 2.5 $CaCl_2$, 5.5 glucose, and 10 HEPES (pH 7.35). The high-K^+ bath solution consisted of (in mM) the following: 150 KCl, 1 $MgCl_2$, 2.5 $CaCl_2$, 5.5 glucose, and 10 HEPES (pH 7.35). The internal solution contained (in mM) 150 KCl, 2 $MgCl_2$, 8.7 $CaCl_2$, 5 HEPES, 10 EGTA (pH 7.2), and 0.3 mg/mL nystatin to create a perforated patch (permeabilizing the cell membrane for ions locally under the patch pipette), plus 5 μg/mL fluorescein (Molecular Probes) to monitor the integrity of the cell in the perforated patch configuration. De- and hyperpolarizing solutions were applied by using a perfusion system. MP recordings on control, depolarized (by high-K^+ buffer) and hyperpolarized (by 10 μM valinomycin) cells are shown in Fig. 1. The resting MP (±SD) was (−30 ± 9) mV, K-HBSS caused depolarization to approximately +5 mV, margatoxin (250 pM) caused depolarization to approximately −5 to 0 mV, and valinomycin resulted in hyperpolarization to approximately (−54 ± 16) mV.

Fluorescence correlation spectroscopy

In a fluorescence correlation spectroscopy (FCS) measurement, a diffraction-limited subfemtoliter volume element of the cell is illuminated by a focused laser beam. Fluorescence fluctuations due to molecules diffusing across the focus are detected, from which the local mobility of the diffusing molecules can be determined. FCS measurements were performed on an Olympus FluoView 1000 confocal microscope equipped with a custom-made two-channel fluorescence spectroscope unit attached to the fourth fluorescence port. The 488 nm line of an Ar ion laser was used to excite Alexa 488, and a 543 nm HeNe laser was used for Cy3, Alexa546, and $DiIC_{18}$; emission was detected through a 514/30 nm bandpass or a 595 nm longpass filter, respectively. Signals from the avalanche photodiodes (single photon-counting module-AQR-13; Perkin-Elmer, Waltham, MA) were fed into an ALV-5000E multiple tau digital correlator card (ALV, Langen, Germany), which calculates the autocorrelation function. 10 × 5 second runs were recorded at three selected points in the membrane of each selected cell. Autocorrelation functions were fitted to a model assuming a single molecular species diffusing in two dimensions:

$$G(\tau) = \frac{1 - T_{tr} + T_{tr}e^{-\tau/\tau_{tr}}}{N(1 - T_{tr})} \times \frac{1}{1 + \tau_d}, \quad (1)$$

where T_{tr} is the fraction of molecules in the triplet state, τ_{tr} is the triplet correlation time, and N is the average number of molecules in the detection volume. The rate of diffusion is characterized by the diffusion time, τ_d, which is the average time that a molecule spends in the illuminated volume. Diffusion coefficients (D) were determined from the following equation:

$$D = \frac{\omega_{xy}^2}{4\tau_d}, \quad (2)$$

where ω_{xy} is the lateral e^{-2} radius of the detection volume. ω_{xy} was calibrated by measuring the diffusion time of 100 nM Alexa 488 or Alexa

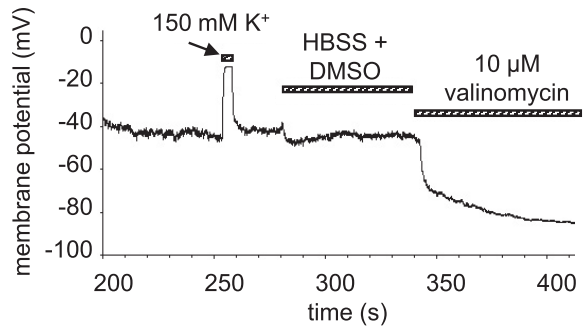

FIGURE 1 Membrane potential changes on K6 cells. Membrane potential was measured by patch clamp with perforated patch configuration. Depolarization was achieved by the high K^+ buffer K-HBSS. K-HBSS was washed out with the perfusion system for repolarization, and then hyperpolarization was induced by valinomycin (10 μM).

546 dyes with known diffusion coefficients (D_{A488} = 414 $\mu m^2/s$, D_{A546} = 341 $\mu m^2/s$ at T = 22.5°C) and substituting them into Eq. 2. Measurements on cells were carried out in eight-well chambered coverglass (Nunc Lab-Tek Thermo Scientific, Waltham, MA) coated with poly-L-lysine (Sigma). Cells were in the de- or hyperpolarizing buffer for maximally 30 min during the measurement. For measuring protein mobility, Fab fragments of the monoclonal antibodies were used with the exception of CD48 and the transferrin receptor, for which whole antibodies were used (IL-2Rα: Alexa 488-anti-Tac Fab, IL-15Rα: Alexa 488-anti-FLAG Fab, MHC I heavy chain: Alexa 488-W6/32 Fab, β2m: Alexa 488-L368 Fab, MHC II/HLA-DR (human leukocyte antigen – antigen D related): Alexa 488-L243 Fab, CD71/transferrin receptor: Alexa 546-MEM75 mAb, CD48 GPI-anchored protein: Cy3-MEM102 mAb).

Fluorescence anisotropy

Labeling with DPH

60 μL of DPH (Sigma-Aldrich) stock solution (1 mg/mL in tetrahydrofuran) was diluted while continuously stirring in HBSS to 1.2 μg/mL and stirred for 1 h. Cells were washed twice and suspended in HBSS (2–3 × 10^6 cells/mL). An equal volume of diluted dye was added to the cell suspension (final DPH concentration was 0.6 μg/mL), and cells were incubated at 37°C for 20 min. Cells were then washed twice and resuspended in the appropriate solution (HBSS, K-HBSS, MgTx in HBSS, 10^6 cells/mL), and their fluorescence anisotropy was measured.

Labeling with TMA-DPH

Cells were washed twice in HBSS and then suspended in HBSS at 2 × 10^6 cells/mL density containing 1.5 μM TMA-DPH (Sigma) and incubated for 5 min at 37°C. Cells were then washed and suspended in the appropriate buffer (10^6 cells/mL) and measured.

MβCD and MβCD/cholesterol treatment

To validate DPH/TMA-DPH anisotropy measurements as an indicator of membrane fluidity, we used methyl-β-cyclodextrin (MβCD; Sigma) and methyl-β-cyclodextrin/cholesterol (MβCD/Chol; Sigma) treated cells. These agents deplete and load cholesterol from or into the cell membrane and make it more fluid or more rigid, respectively. Cells were washed twice in HBSS and then incubated with MβCD (two samples with different concentrations: 5 mM for 45 min and 3 mM for 30 min at 37°C) or MβCD/Chol (1.5 mg/mL for 60 min at 37°C). After treatment, cells were washed and stained with DPH or TMA-DPH, as described above.

Fluorescence anisotropy measurements

Anisotropy measurements were carried out on a Jobin Yvon FluoroLog-3 spectrofluorimeter equipped with dual path excitation and emission monochromators and a cooled photomultiplier tube. The intensity of the Xe lamp was monitored by a reference photomultiplier tube and was used for correcting excitation intensity fluctuations. Steady-state fluorescence anisotropy values were obtained by measuring the fluorescence intensities I_{VV} and I_{VH} (excitation: 355 nm, emission: 430 nm, band width 5 nm) in a 100 μL quartz cuvette with 2 × 5 mm windows (Hellma Analytics, Plainview, NY). Indexes VV and VH indicate the vertical-vertical or vertical-horizontal orientation of the excitation and emission polarizers, respectively. Unstained cells having equal cell densities as the samples were measured for autofluorescence correction of the fluorescence intensities measured at different polarizer settings. A correction factor for the unequal transmission of horizontally and vertically polarized light components by the optical elements ($G = I_{HV}/I_{HH}$) was also determined and used for calculating the fluorescence anisotropy as follows:

$$r = \frac{I_{VV} - GI_{VH}}{I_{VV} + 2GI_{VH}}. \quad (3)$$

Förster resonance energy transfer

Homo- and heteroassociations of membrane proteins were assessed by Förster resonance energy transfer (FRET) as described (29). Cells were doubly labeled with donor- (Alexa 546) and acceptor-tagged (Alexa 647) antibodies targeting the investigated proteins. Measurements were carried out on a FACSAria III instrument (Becton Dickinson, Franklin Lakes, NJ). Three fluorescence intensities (I_1: donor, I_2: FRET, and I_3: acceptor channel) were detected from each cell at the following excitation wavelengths and detection bands: 561/595 ± 25, 561/>635, and 633/>635 nm. Spectral bleed-through factors S_1, S_2, and S_3 and the α-factor defining the relative detection efficiencies of the acceptor to the donor were determined from samples singly labeled with donor or acceptor antibodies. Dead cells were excluded from the analysis based on side scatter versus forward scatter dot plots. FRET data were analyzed with a custom-written software called ReFlex (30). From the three detected intensities, the mean FRET efficiency, E, was determined for each cell. Results were presented as geometric means of cell-by-cell E histograms.

Signal transduction

Binding of IL-2 or -15 to their receptors activates the protein tyrosine kinases Jak1 and Jak3, which associate with and phosphorylate the IL-2/15R β- and γ_c-chains. These phosphotyrosine motifs dock STAT3 and STAT5, which also become phosphorylated by the Jaks. To assess the efficiency of cytokine signaling at different MPs, we detected phosphorylated STAT5 with anti-phospho-STAT5 mAb (Tyr694). Before cytokine treatment, cells were deprived of IL-2 for 24–48 h. We measured the time and cytokine concentration dependence of STAT5 phosphorylation on K6 and FT7.10 cells and chose conditions in which phosphorylation was not in saturation at resting MP. This way, we could detect either an increase or a decrease of phosphorylation upon de- or hyperpolarization relative to the control. These conditions meant 10 min incubation with 50 pM IL-2 (Hoffmann-La Roche) or 5 min with 50 pM IL-15 (Biopharmaceutical Development Program, National Cancer Institute at Frederick) at 37°C. After cytokine treatment, cells were fixed with 2% formaldehyde (Scharlab, Debrecen, Hungary) for 10 min at 37°C, permeabilized (90% methanol for 30 min on ice), and labeled with Alexa647-conjugated anti-pSTAT5 antibody (BD Biosciences, San Jose, CA) for 40 min at room temperature. Nonspecific binding of anti-PSTAT5 was detected from a sample incubated with the isotype control antibody (provided by the manufacturer). Measurements were carried out on a Becton Dickinson FACSArray (excitation: 632 nm, detection: 661/16 nm) or FACSAria III (excitation: 633 nm, detection: >635 nm) flow cytometer. The ReFlex or FCS Express (De Novo Software, Glendale, CA) software programs were used to analyze data from >10,000 cells per sample.

Prediction of hydrophobicity of membrane proteins

Hydrophobicity analysis and determination of the TMR were performed by the software "TMMOD: Hidden Markov Model for Transmembrane Protein Topology Prediction" (http://liao.cis.udel.edu/website/servers/TMMOD (31)) or taken from the UniProt database (http://www.uniprot.org).

Statistical analysis

Means were compared using an unpaired t-test with Welch correction, through which we found unequal variances.

RESULTS

Mobility of membrane proteins measured by FCS

Protein mobility may depend on several factors, such as the size of the molecular complex in which it resides, the local

microviscosity/friction, and attachment to different cellular components. Changes in the MP may affect the conformation of membrane proteins and thereby influence their interactions with other membrane constituents. On the other hand, the MP may also influence the general properties of the cell membrane (microviscosity, thickness). Through these changes, the MP may also modulate receptor function.

We measured the mobility of IL-2 and IL-15 receptor α-subunits, MHC I heavy and light chains (β2-microglobulin), and MHC II molecules in resting, depolarized (via high-K^+ K-HBSS buffer or margatoxin), and hyperpolarized (via valinomycin) cells. Averaged autocorrelation curves of IL-2Rα are shown in Fig. 2, *J* and *K*. The curve was shifted to the right toward longer diffusion times upon

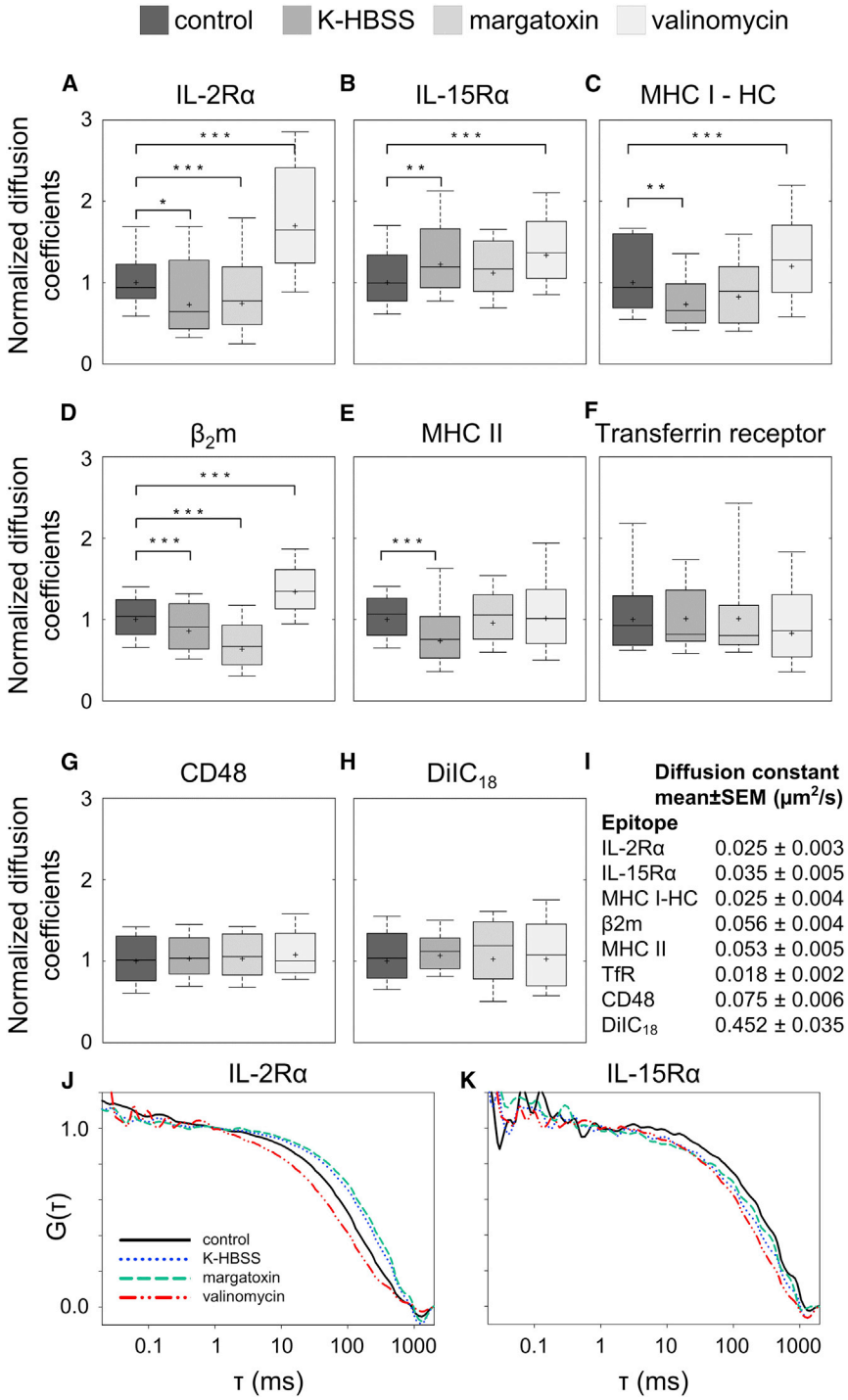

FIGURE 2 Dependence of FCS-determined diffusion coefficients of membrane components on the membrane potential (*A–I*). All measurements were carried out on K6 cells except with IL-15Rα, which was measured on FT7.10 cells. Control samples were incubated in HBSS, and depolarization was achieved by K-HBSS buffer or by margatoxin (1.5 nM); hyperpolarization was induced by valinomycin (10 μM). (*A–H*) *D* values were normalized to the geometric mean (marked by *asterisk*) measured at resting MP; the horizontal line marks the median, the boxes denote the 25 and 75 percentile values, and the whiskers indicate the 10 and 90 percentile values. (*I*) Geometric mean of *D* and SEs are shown (n: 32–207 cells/treatment). Statistically significant changes relative to the control sample are marked as $*p < 0.05$, $**p < 0.01$, and $***p < 0.001$. (*J* and *K*) Autocorrelation functions of IL-2Rα and IL-15Rα are shown (tagged by Alexa488-anti-Tac Fab and Alexa488-anti-FLAG Fab). The curves shown are the averages of normalized autocorrelation curves for n = 14–20 cells per treatment. To see this figure in color, go online.

depolarization with K-HBSS, implying a decrease of mobility, and an opposing change was detected upon hyperpolarization. The reduction of mobility upon depolarization is clearly reflected by the significant decrease of the diffusion coefficient, *D* (Fig. 2 *A*), both in the case of K-HBSS and of MgTx. A similar decrease of *D* can also be observed for the MHC I heavy and light chains and for MHC II to different extents for the different proteins (Fig. 2, *C–E*). Contrary to this, hyperpolarization resulted in an increase of diffusion coefficients for IL-2Rα and MHC I. Interestingly, IL-15Rα behaved differently; its *D* value increased after both depolarizing and hyperpolarizing treatments (Fig. 2 *B*).

The above molecules are transmembrane proteins known to be enriched in lipid rafts. To check whether MP changes alter the mobility of other membrane components as well, we measured the mobility of CD48 (a GPI-anchored protein), $DiIC_{18}(3)$ (a fluorescent lipid analog with saturated fatty acid tails)—both of which are enriched in lipid rafts (22,23)—and transferrin receptor (TfR), which is enriched in coated pits (24). For these molecules, neither depolarization nor hyperpolarization induced any considerable change of mobility (Fig. 2, *F–H*).

Membrane fluidity does not change upon membrane depolarization

Changes in the mobility of membrane proteins may result from a generic change of membrane fluidity. To monitor membrane fluidity, we measured the fluorescence anisotropy of DPH and TMA-DPH membrane probes. DPH is located at the fatty acid tail region of the lipid bilayer, whereas TMA-DPH, due to its positive charge, is enriched in the inner leaflet of the membrane. Anisotropy measures the rotational mobility of the lipid probe and is an indicator of the local viscosity or fluidity of the cell membrane. The anisotropy of neither probe changed significantly upon depolarization of K6 cells with K-HBSS or margatoxin (Table 2). Therefore, we can exclude the possibility that membrane depolarization exerts its effect on protein mobility via changing membrane fluidity. To check the sensitivity of anisotropy measurements to changes of membrane fluidity, we depleted or enriched membrane cholesterol by treatment with MβCD or cholesterol-loaded MβCD, respectively. The anisotropy of both probes decreased significantly in cholesterol-depleted cells, implying that the membrane fluidity increased. Contrary to this, the anisotropy increased in cholesterol-loaded cells, suggesting a decrease of membrane fluidity. Similar results were obtained for FT7.10 cells (data not shown).

TABLE 2 Fluorescence Anisotropy Values of the Two Membrane Probes DPH and TMA-DPH Measured on K6 Cells

CELL	TREATMENT	r (DPH)	r(TMA-DPH)
K6	control	0.171 ± 0.001	0.2635 ± 0.0001
	50% K-HBSS	0.173 ± 0.001	0.2656 ± 0.0006
	K-HBSS	0.179 ± 0.0004	0.2626 ± 0.0001
K6	control	0.1804 ± 0.0006	0.2540 ± 0.0003
	margatoxin	0.1790 ± 0.0003	0.2554 ± 0.0004
K6	control	0.1998 ± 0.0005	0.2541 ± 0.0003
	MβCD 3 mM 30′	0.1771 ± 0.0009***	0.2268 ± 0.0009***
	MβCD 5 mM 45′	0.1576 ± 0.0003***	0.2259 ± 0.0050***
	MβCD/chol. 1.5 mg/mL 60′	0.2607 ± 0.0002***	0.2717 ± 0.0016***

Data are derived from two independent experiments. ***$p < 0.0001$.

Assessment of protein homo- and heteroassociations by FRET

Another possible reason for the detected shifts in protein mobility could be a change in their homo- or heterotypic clustering patterns. We monitored molecular proximities between the studied membrane proteins by flow cytometric cell-by-cell FRET measurements. In Fig. 3, the average FRET efficiencies resulting from homotypic (*A*) and heterotypic associations (*B*) are shown at different MPs. In Fig. S1, cell-by-cell donor and acceptor intensity histograms and FRET efficiency histograms are also presented for selected donor-acceptor pairs. The FRET efficiency increases with

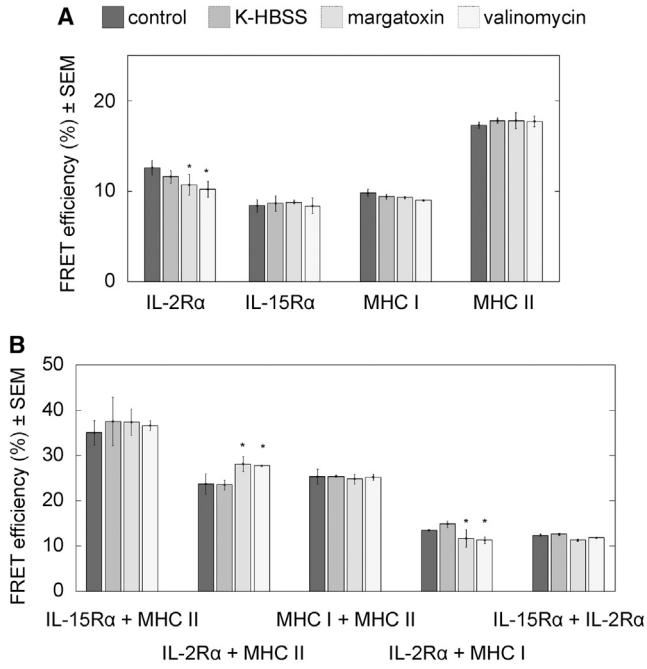

FIGURE 3 Homoassociations (*A*) and heteroassociations of (*B*) of IL-2Rα, IL-15Rα, MHC I, and MHC II detected by flow cytometric FRET measurements on FT7.10 cells. Receptors were labeled with donor-tagged (Alexa 546) and acceptor-tagged (Alexa 647) mAbs. The average FRET efficiencies from three independent experiments are shown; in each experiment, >10,000 cells were measured per treatment. Control samples were incubated in HBSS, and depolarization was achieved either by K-HBSS buffer or by margatoxin (1.5 nM); hyperpolarization was induced by valinomycin (10 μM). Statistically significant changes relative to the control sample are marked as *$p < 0.05$. Histograms of donor and acceptor intensity are shown; FRET efficiency as well as the dependence of FRET efficiency on the acceptor expression level is shown in Fig. S1.

the increase of acceptor-tagged protein expression level, as expected according to the law of mass action (Fig. S1). FRET efficiencies characterizing homoassociations of IL-15Rα, MHC I, or MHC II did not change significantly upon either de- or hyperpolarization (Fig. 3 *A*). The only statistically significant changes were observed in the case of IL-2Rα, where *E* decreased slightly by ~3% upon hyperpolarization and by 2% upon margatoxin treatment. We also tested the heteroassociations between selected pairs of IL-2Rα, IL-15Rα, MHC I, and MHC II (Fig. 3 *B*). In most cases, we did not observe any significant change in the FRET efficiencies with the exception of the IL-2Rα + MHC I pair. For this pair of proteins, *E* increased by ~4% upon depolarization with margatoxin and also upon hyperpolarization with valinomycin. Altogether, our FRET data suggest that changes in the homotypic or heterotypic associations (at least the ones studied) probably cannot account for the observed significant decrease of mobility upon depolarization and increase upon hyperpolarization for the studied membrane proteins.

Depolarization and hyperpolarization have distinct effects on IL-2- and IL-15-induced signaling

The effect of MP on the efficiency of cytokine signaling was monitored by measuring IL-2- and IL-15-induced STAT5 phosphorylation on K6 and FT7.10 cells, respectively. The K_d of IL-2 and IL-15 to their high-affinity heterotrimeric (IL-2R$\alpha\beta\gamma_c$ or IL-15R$\alpha\beta\gamma_c$) receptors is 10 pM, whereas that of the intermediate affinity $\beta\gamma_c$-heterodimers is 1 nM (1). To target only the high affinity receptors on the cells, we used 50 pM cytokine concentration, at which cytokines nearly saturate the high-affinity heterotrimers but do not significantly bind to intermediate affinity heterodimers. This allows us to study signaling via the cytokine-specific high-affinity heterotrimers separately. The PSTAT5 intensities were determined on a cell-by-cell basis by flow cytometry by using Alexa647-anti-PSTAT5 mAbs. Cells not treated with cytokine gave single peaks in the PSTAT5 histograms representing the basal level of STAT5 phosphorylation; the average normalized PSTAT5 signals are shown in the third columns of Fig. 4, *A* and *B*. After cytokine treatment, we found two cell populations, a responding (high PSTAT5) and a nonresponding (low PSTAT5) population for both IL-2 and IL-15 (Fig. S2). Fig. 4 shows the average PSTAT5 signals of the responding populations, normalized to the signal of the cytokine-treated control cells at resting MP. Depolarization by K-HBSS or by margatoxin caused a moderate but statistically significant increase in IL-2-induced STAT5 phosphorylation as compared to cells at resting MP, whereas hyperpolarization by valinomycin had no significant effect. Contrary to this, IL-15-induced phosphorylation was not significantly affected by depolarization, whereas hyperpolarization evoked a significant decrease relative to the control. These data indicate that depolarization and hyperpolarization affect signaling by IL-2 and IL-15 in distinct ways.

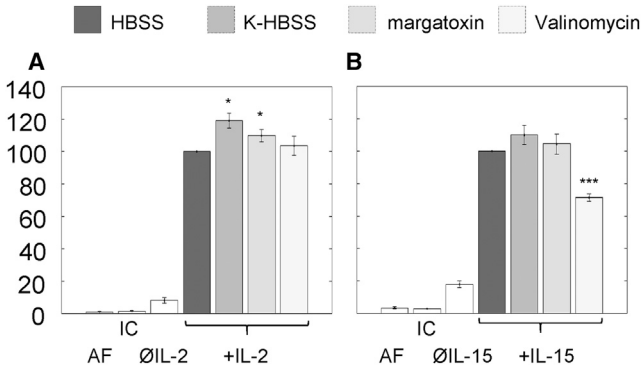

FIGURE 4 Signaling efficiency of IL-2 and -15 receptors. Flow cytometry was used to measure STAT5 phosphorylation on a cell-by-cell basis using Alexa647-anti-PSTAT mAbs. Control samples were incubated in HBSS, and depolarization was achieved either by K-HBSS buffer or by margatoxin (1.5 nM); hyperpolarization was induced by valinomycin (10 μM). (*A*) K6 cells were stimulated with IL-2 (50 pM, 10 min, 37°C). (*B*) FT7.10 cells were treated with IL-15 (50 pM, 5 min, 37°C). Data from labeled samples were corrected with the mean fluorescence of the isotype controls (IC) and normalized to the intensities measured at resting MP. Autofluorescence (AF) is also shown. The third columns (ØIL-2, ØIL-15) display the normalized basal STAT5 phosphorylation in the absence of cytokine. Averages ± SEM of n = 6 independent measurements are presented. Statistically significant changes relative to the control sample are marked as $*p < 0.05$ and $***p < 0.001$. Gating strategies and histograms of cell-by-cell PSTAT5 distributions are shown in Fig. S2.

DISCUSSION

The MP has three components: the transmembrane potential (due to the unequal distribution of ions on the two sides of the membrane), the surface potential (arising from the incomplete neutralization of the charged head groups of lipids), and the dipole potential (generated by the ordered orientation of lipid carbonyl and membrane-attached water dipole moments) (32). Regulation of the MP by ion channel activity plays an important role during the activation of T lymphocytes (33,34). Upon activation, Ca^{2+} entry depolarizes the plasma membrane, and K^+ efflux through voltage-gated Kv1.3 and Ca^{2+}-regulated KCa3.1 channels is necessary to restore and maintain the negative MP needed for prolonged Ca^{2+} entry and subsequent T cell proliferation. Elevated extracellular K^+ level and opening of Kv1.3 channels were found to activate T cell β1-integrin moieties and to induce integrin-mediated adhesion and migration (35).

Transitions between functional states are well-known features of voltage gated ion channels, which possess electrically charged voltage-sensing domains that move relative to the membrane as the MP changes (36,37). The high electric field in the plasma membrane might also influence the conformation of other kinds of membrane proteins having an uneven charge distribution, such as a permanent or

induced dipole moment or a net electric charge. Thereby, interactions and activity of membrane proteins may also be modulated by the MP. Earlier FRET experiments indicated that the conformation of the MHC I protein altered reversibly upon membrane depolarization (38). Recently, the dipole potential in the plasma membrane was shown to affect the association and signaling of erbB receptor tyrosine kinases (39).

We set out to determine the dependence of the biophysical properties and signaling efficiency of IL-2 and IL-15 receptors on the value of the MP. We investigated the mobility of IL-2/15 receptor subunits and MHC glycoproteins on resting, depolarized cells as well as in hyperpolarized cells by FCS. The applied treatments modified the transmembrane potential. The mobility of IL-2Rα, MHC I, and MHC II decreased significantly upon membrane depolarization, whereas that of IL-15Rα increased. The question arises of whether the depolarization-induced decrease of mobility is specific to the investigated proteins, to transmembrane proteins in general, or to all components of the plasma membrane. As controls, we tested the mobility of the lipid raft-associated GPI-anchored protein CD48 which has no transmembrane peptide chain, the nonraft transmembrane transferrin receptor, and the lipid analog $DiIC_{18}$; we found no significant changes in the mobility of these molecules upon changes of the MP. We can conclude that out of the molecules investigated by us, only raft-localized transmembrane proteins slowed down or became more mobile upon depolarization.

We can speculate that changes of protein mobility evoked by MP changes might be related to the number and distribution of charged residues near the TMRs of these molecules. We analyzed the charges of the 10 amino acids flanking the TMRs on both sides in the studied transmembrane proteins (see the Supporting Material). IL-2Rα, IL-15Rα, HLA A, HLA DR, and TfR all contain positive charges in their cytoplasmic flanks in accordance with the positive-inside rule (20). The extracellular flanks either carry a net negative charge (IL-2Rα, HLA DR), as suggested by the negative-not-inside/negative-outside rule (21), or a net zero charge (IL-15Rα, HLA A), with the exception of the TfR, which has three positive charges at this region. There is an interesting correlation between the charges of the flanking regions and changes in protein mobility upon changes of MP: the largest changes in mobility occurred for IL-2Rα and MHC I, which had the highest number of positive residues (6 and 5, respectively) in the cytoplasmic flanks. On the other hand, the mobility of TfR did not change upon de- or hyperpolarization; this protein has two positive residues in the cytoplasmic flank and three positive residues in the extracellular flank, resulting in a less skewed, more balanced charge distribution (lower or no dipole moment across the membrane) than those of the other studied proteins. Our hypothesis that the charge distribution of the TMR-flanking regions plays a role in regulating the mobility of transmembrane proteins at different MPs requires further investigation.

As another control, we also checked whether a general property, i.e., membrane fluidity, might cause the observed changes in mobility. Therefore, we measured the fluorescence anisotropy of the DPH and TMA-DPH membrane probes reflecting their rotational mobility. We could exclude the change of fluidity as an explanation because the anisotropies did not change significantly upon depolarization.

The lipid membrane itself has a nonuniform charge distribution; thus, its thickness changes at different MPs because of electrostriction (40). The membrane becomes thinner if the absolute value of the MP is larger (hyperpolarization) and thicker when depolarized to 0 mV. This may influence the interacting surface area between the lipid bilayer and a membrane protein; therefore, it may affect friction and protein mobility. We can estimate the order of magnitude of the change of membrane thickness as follows:

$$\Delta h = -C_S V^2 / (2E_\perp), \tag{4}$$

where Δh is the change in membrane thickness at an MP of V (relative to 0 mV), C_S is the specific capacitance of the cell membrane (taken to be 1.2 μF/cm^2 (41)), and $E_\perp$ is Young's modulus of elasticity perpendicular to the membrane surface (taken to be $\sim$20 N/cm^2 for a lipid bilayer (42)). Substituting $V = -50$ mV into Eq. 4 yields $\Delta h \sim 0.75$ Å, which is $\sim$1% of the thickness of the plasma membrane (5–10 nm). Such a small change is improbable to explain the changes of protein mobility observed upon altering the MP.

Changes of clustering properties could also be a reason for altered protein mobility. FRET measurements assessing homo- and heteroassociations between IL-2Rα, IL-15Rα, and MHC I and II molecules showed that there was just a slight variation in the clustering properties of these proteins, which probably cannot account for the detected significant alterations of protein mobilities.

Because IL-2Rα and MHC I can interact with the cytoskeleton (12,43), changes in cytoskeletal organization upon de- or hyperpolarization could also be considered as a mechanism explaining the observed changes of membrane protein mobility. In bovine corneal endothelial cells, membrane depolarization induced redistribution of F-actin toward the cell interior, whereas hyperpolarization provoked a compaction of adherens junction-associated actin filaments toward the plasma membrane and an increase in the stability of the adherens junctions (44–46). However, such changes in cytoskeletal reorganization do not seem to provide a plausible explanation for our observations on protein mobility; redistribution of actin toward the cell interior (from the periphery) on depolarization should rather decrease the possibility of interactions of the actin cytoskeleton with membrane proteins and result in an increase of

protein mobility, contrary to our observations. However, we cannot exclude the possibility that in human T cells, the cytoskeleton might react to MP changes in a different manner.

On the other hand, MP changes induced significant changes in receptor activity according to our signal transduction measurements. The signaling capability of IL-2R was increased upon depolarization, whereas the signaling efficiency of IL-15R decreased upon hyperpolarization. These results show that the MP influences signaling by IL-2 and -15 in distinct ways, which could be related to the antagonistic functions of the two cytokines. IL-2Rα and IL-15Rα may differentially interact with the signaling β- and γ-subunits and, perhaps due to their different charge distributions, modify their conformations in distinct ways at different MPs, which could be the reason for the distinct changes of IL-2- versus IL-15-induced signaling under depolarizing and hyperpolarizing conditions. The lowered mobility of IL-2R upon depolarization could also enhance the formation of signaling complexes, which would be in line with the detected increase of IL-2-induced STAT5 phosphorylation.

Regulatory T cells (T_{reg} cells) express IL-2R abundantly. IL-2-dependent activation of STAT5 has an essential role in their suppressor function, limiting the activation of $CD8^+$ antitumor effector T cells (47). A hypoxic/necrotic tumor microenvironment with excess extracellular K^+ can depolarize T_{reg} cells, thus enhancing their IL-2-induced STAT5 activation, which could in turn contribute to the impairment of tumor surveillance by effector T cells. The tumor microenvironment also influences T cell effector function in a more direct way. The enhanced $[K^+]_e$ leads to an elevation of intracellular $[K^+]_i$ in effector T cells, which impairs T-cell-receptor-driven Akt-mTOR phosphorylation and effector programs, independent of the MP (14). The somewhat different influence on the IL-2-induced STAT5 phosphorylation of high $[K^+]_e$ and margatoxin might suggest that factors other than the MP, such as $[K^+]_i$, might also play a role in regulating the efficiency of phosphorylation.

The importance of the ion milieu and MP changes in a T cell's life is now unquestionable. The next step in understanding these effects is to unveil how a change in the MP can affect the conformation of the different components of the cell membrane and how exactly it can modify their function. It seems plausible that MP changes can be used by cells to control their life processes in delicate ways. Our results may contribute to understanding how this complex and sensitive sensor and regulating system connecting the extra- and intracellular space functions.

SUPPORTING MATERIAL

Supporting Materials and Methods and two figures are available at http://www.biophysj.org/biophysj/supplemental/S0006-3495(18)30533-2.

AUTHOR CONTRIBUTIONS

É.N., G.M., V.S., J.V., and G.V. carried out and analyzed most experiments with contributions from F.P. F.P. analyzed the protein sequences. É.N., V.S., and G.V. wrote the article with input from K.T., S.D., G.P., T.A.W., and A.B. S.D., G.P., and G.V. conceived the experiments.

ACKNOWLEDGMENTS

We dedicate this work to the memory of our dear friend, Prof. Jörg Langowski, who was a pioneer in the development of FCS and its application in cell biology. We thank Ágota Csóti for testing the efficiency of K^+ channel blockers, Dr. Péter Hajdú for useful discussions, and Edina Nagy and Rita Utasi-Szabó for excellent technical assistance.

Financial support was provided by GINOP-2.3.2-15-2016-00026, GINOP-2.3.3-15-2016-00003, GINOP-2.3.3-15-2016-00030, K103965 (to G.V.), EFOP-3.6.1-16-2016-00022 and K119417 (to G.P.) from the National Research, Development and Innovation Office, Hungary; TÁMOP-4.2.4.A/2-11/1-2012-0001 from the "National Excellence Program" (to G.V.); EFOP-3.6.3-VEKOP-16-2017-00009 co-financed by the European Union and the European Social Found (to A.B. and G.V.); the German Academic Exchange Service #57391835 and the Tempus Public Foundation #273478 (to G.V. and K.T.); and the intramural research program of the National Cancer Institute, National Institutes of Health (to T.A.W.).

REFERENCES

1. Fehniger, T. A., M. A. Cooper, and M. A. Caligiuri. 2002. Interleukin-2 and interleukin-15: immunotherapy for cancer. *Cytokine Growth Factor Rev.* 13:169–183.
2. Waldmann, T. A. 2006. The biology of interleukin-2 and interleukin-15: implications for cancer therapy and vaccine design. *Nat. Rev. Immunol.* 6:595–601.
3. Waldmann, T. A., S. Dubois, and Y. Tagaya. 2001. Contrasting roles of IL-2 and IL-15 in the life and death of lymphocytes: implications for immunotherapy. *Immunity.* 14:105–110.
4. Germain, R. N. 1994. MHC-dependent antigen processing and peptide presentation: providing ligands for T lymphocyte activation. *Cell.* 76:287–299.
5. Damjanovich, S., L. Bene, …, T. A. Waldmann. 1997. Preassembly of interleukin 2 (IL-2) receptor subunits on resting Kit 225 K6 T cells and their modulation by IL-2, IL-7, and IL-15: a fluorescence resonance energy transfer study. *Proc. Natl. Acad. Sci. USA.* 94:13134–13139.
6. Matko, J., A. Bodnar, …, S. Damjanovich. 2002. GPI-microdomains (membrane rafts) and signaling of the multi-chain interleukin-2 receptor in human lymphoma/leukemia T cell lines. *Eur. J. Biochem.* 269:1199–1208.
7. Mocsár, G., J. Volkó, …, G. Vámosi. 2016. MHC I expression regulates co-clustering and mobility of interleukin-2 and -15 receptors in T cells. *Biophys. J.* 111:100–112.
8. Vámosi, G., A. Bodnár, …, S. Damjanovich. 2004. IL-2 and IL-15 receptor alpha-subunits are coexpressed in a supramolecular receptor cluster in lipid rafts of T cells. *Proc. Natl. Acad. Sci. USA.* 101:11082–11087.
9. Vereb, G., J. Matkó, …, S. Damjanovich. 2000. Cholesterol-dependent clustering of IL-2Ralpha and its colocalization with HLA and CD48 on T lymphoma cells suggest their functional association with lipid rafts. *Proc. Natl. Acad. Sci. USA.* 97:6013–6018.
10. Nizsaloczki, E., I. Csomos, …, A. Bodnar. 2014. Distinct spatial relationship of the interleukin-9 receptor with interleukin-2 receptor and major histocompatibility complex glycoproteins in human T lymphoma cells. *Chemphyschem.* 15:3969–3978.

11. Surls, J., C. Nazarov-Stoica, …, T. D. Brumeanu. 2012. Increased membrane cholesterol in lymphocytes diverts T-cells toward an inflammatory response. *PLoS One*. 7:e38733.
12. Pillet, A. H., V. Lavergne, …, T. Rose. 2010. IL-2 induces conformational changes in its preassembled receptor core, which then migrates in lipid raft and binds to the cytoskeleton meshwork. *J. Mol. Biol.* 403:671–692.
13. Kurgonaite, K., H. Gandhi, …, C. Bökel. 2015. Essential role of endocytosis for interleukin-4-receptor-mediated JAK/STAT signalling. *J. Cell Sci.* 128:3781–3795.
14. Eil, R., S. K. Vodnala, …, N. P. Restifo. 2016. Ionic immune suppression within the tumour microenvironment limits T cell effector function. *Nature*. 537:539–543.
15. Chimote, A. A., Z. Kuras, and L. Conforti. 2012. Disruption of kv1.3 channel forward vesicular trafficking by hypoxia in human T lymphocytes. *J. Biol. Chem.* 287:2055–2067.
16. Caldwell, C. C., H. Kojima, …, M. V. Sitkovsky. 2001. Differential effects of physiologically relevant hypoxic conditions on T lymphocyte development and effector functions. *J. Immunol.* 167:6140–6149.
17. Brown, J. M. 2000. Exploiting the hypoxic cancer cell: mechanisms and therapeutic strategies. *Mol. Med. Today.* 6:157–162.
18. Vuillefroy de Silly, R., P. Y. Dietrich, and P. R. Walker. 2016. Hypoxia and antitumor $CD8^+$ T cells: an incompatible alliance? *OncoImmunology.* 5:e1232236.
19. Lewis, J. S., J. A. Lee, …, C. E. Lewis. 1999. Macrophage responses to hypoxia: relevance to disease mechanisms. *J. Leukoc. Biol.* 66:889–900.
20. Boyd, D., and J. Beckwith. 1990. The role of charged amino acids in the localization of secreted and membrane proteins. *Cell.* 62:1031–1033.
21. Baker, J. A., W. C. Wong, …, F. Eisenhaber. 2017. Charged residues next to transmembrane regions revisited: "positive-inside rule" is complemented by the "negative inside depletion/outside enrichment rule". *BMC Biol.* 15:66.
22. Moran, M., and M. C. Miceli. 1998. Engagement of GPI-linked CD48 contributes to TCR signals and cytoskeletal reorganization: a role for lipid rafts in T cell activation. *Immunity.* 9:787–796.
23. Gombos, I., G. Steinbach, …, J. Matkó. 2008. Some new faces of membrane microdomains: a complex confocal fluorescence, differential polarization, and FCS imaging study on live immune cells. *Cytometry A.* 73:220–229.
24. Iacopetta, B. J., S. Rothenberger, and L. C. Kühn. 1988. A role for the cytoplasmic domain in transferrin receptor sorting and coated pit formation during endocytosis. *Cell.* 54:485–489.
25. Hori, T., T. Uchiyama, …, H. Uchino. 1987. Establishment of an interleukin 2-dependent human T cell line from a patient with T cell chronic lymphocytic leukemia who is not infected with human T cell leukemia/lymphoma virus. *Blood.* 70:1069–1072.
26. Bartok, A., A. Toth, …, Z. Varga. 2014. Margatoxin is a non-selective inhibitor of human Kv1.3 K+ channels. *Toxicon.* 87:6–16.
27. Rose, M. C., and R. W. Henkens. 1974. Stability of sodium and potassium complexes of valinomycin. *Biochim. Biophys. Acta.* 372: 426–435.
28. Hodgkin, A. L., and B. Katz. 1949. The effect of sodium ions on the electrical activity of giant axon of the squid. *J. Physiol.* 108:37–77.
29. Sebestyén, Z., P. Nagy, …, J. Szöllosi. 2002. Long wavelength fluorophores and cell-by-cell correction for autofluorescence significantly improves the accuracy of flow cytometric energy transfer measurements on a dual-laser benchtop flow cytometer. *Cytometry.* 48:124–135.
30. Szentesi, G., G. Horváth, …, L. Mátyus. 2004. Computer program for determining fluorescence resonance energy transfer efficiency from flow cytometric data on a cell-by-cell basis. *Comput. Methods Programs Biomed.* 75:201–211.
31. Kahsay, R. Y., G. Gao, and L. Liao. 2005. An improved hidden Markov model for transmembrane protein detection and topology prediction and its applications to complete genomes. *Bioinformatics.* 21:1853–1858.
32. O'Shea, P. 2003. Intermolecular interactions with/within cell membranes and the trinity of membrane potentials: kinetics and imaging. *Biochem. Soc. Trans.* 31:990–996.
33. Cahalan, M. D., and K. G. Chandy. 2009. The functional network of ion channels in T lymphocytes. *Immunol. Rev.* 231:59–87.
34. Panyi, G., G. Vámosi, …, S. Damjanovich. 2004. Looking through ion channels: recharged concepts in T-cell signaling. *Trends Immunol.* 25:565–569.
35. Levite, M., L. Cahalon, …, O. Lider. 2000. Extracellular K(+) and opening of voltage-gated potassium channels activate T cell integrin function: physical and functional association between Kv1.3 channels and beta1 integrins. *J. Exp. Med.* 191:1167–1176.
36. Catterall, W. A. 2010. Ion channel voltage sensors: structure, function, and pathophysiology. *Neuron.* 67:915–928.
37. Swartz, K. J. 2008. Sensing voltage across lipid membranes. *Nature.* 456:891–897.
38. Bene, L., J. Szöllősi, …, S. Damjanovich. 1997. Major histocompatibility complex class I protein conformation altered by transmembrane potential changes. *Cytometry.* 27:353–357.
39. Kovács, T., G. Batta, …, P. Nagy. 2016. The dipole potential modifies the clustering and ligand binding affinity of ErbB proteins and their signaling efficiency. *Sci. Rep.* 6:35850.
40. Hianik, T., J. Dlugopolsky, …, S. A. Ivanov. 1996. Electrostriction and membrane potential of lipid bilayers on a metal support. *Colloid Surf. A Physicochem. Eng. Asp.* 106:109–118.
41. Huang, Y., X. B. Wang, …, F. F. Becker. 1999. Membrane dielectric responses of human T-lymphocytes following mitogenic stimulation. *Biochim. Biophys. Acta.* 1417:51–62.
42. Sabotin, I., A. M. Lebar, …, P. Kramar. 2009. Measurement protocol for planar lipid bilayer viscoelastic properties. *IEEE Trans. Dielectr. Electr. Insul.* 16:1236–1242.
43. Lavi, Y., N. Gov, …, L. A. Gheber. 2012. Lifetime of major histocompatibility complex class-I membrane clusters is controlled by the actin cytoskeleton. *Biophys. J.* 102:1543–1550.
44. Chifflet, S., V. Correa, …, J. A. Hernández. 2004. Effect of membrane potential depolarization on the organization of the actin cytoskeleton of eye epithelia. The role of adherens junctions. *Exp. Eye Res.* 79:769–777.
45. Chifflet, S., J. A. Hernández, …, A. Cirillo. 2003. Nonspecific depolarization of the plasma membrane potential induces cytoskeletal modifications of bovine corneal endothelial cells in culture. *Exp. Cell Res.* 282:1–13.
46. Nin, V., J. A. Hernández, and S. Chifflet. 2009. Hyperpolarization of the plasma membrane potential provokes reorganization of the actin cytoskeleton and increases the stability of adherens junctions in bovine corneal endothelial cells in culture. *Cell Motil. Cytoskeleton.* 66:1087–1099.
47. Chinen, T., A. K. Kannan, …, A. Y. Rudensky. 2016. An essential role for the IL-2 receptor in T_{reg} cell function. *Nat. Immunol.* 17:1322–1333.
48. Uchiyama, T., S. Broder, and T. A. Waldmann. 1981. A monoclonal antibody (anti-Tac) reactive with activated and functionally mature human T cells. I. Production of anti-Tac monoclonal antibody and distribution of Tac (+) cells. *J. Immunol.* 126:1393–1397.
49. Barnstable, C. J., W. F. Bodmer, …, A. Ziegler. 1978. Production of monoclonal antibodies to group A erythrocytes, HLA and other human cell surface antigens-new tools for genetic analysis. *Cell.* 14:9–20.
50. Lampson, L. A., C. A. Fisher, and J. P. Whelan. 1983. Striking paucity of HLA-A, B, C and beta 2-microglobulin on human neuroblastoma cell lines. *J. Immunol.* 130:2471–2478.
51. Brodsky, F. M. 1984. A matrix approach to human class II histocompatibility antigens: reactions of four monoclonal antibodies with the products of nine haplotypes. *Immunogenetics.* 19:179–194.

Biophysical Journal, Volume *114*

Supplemental Information

Membrane Potential Distinctly Modulates Mobility and Signaling of IL-2 and IL-15 Receptors in T Cells

Éva Nagy, Gábor Mocsár, Veronika Sebestyén, Julianna Volkó, Ferenc Papp, Katalin Tóth, Sándor Damjanovich, György Panyi, Thomas A. Waldmann, Andrea Bodnár, and György Vámosi

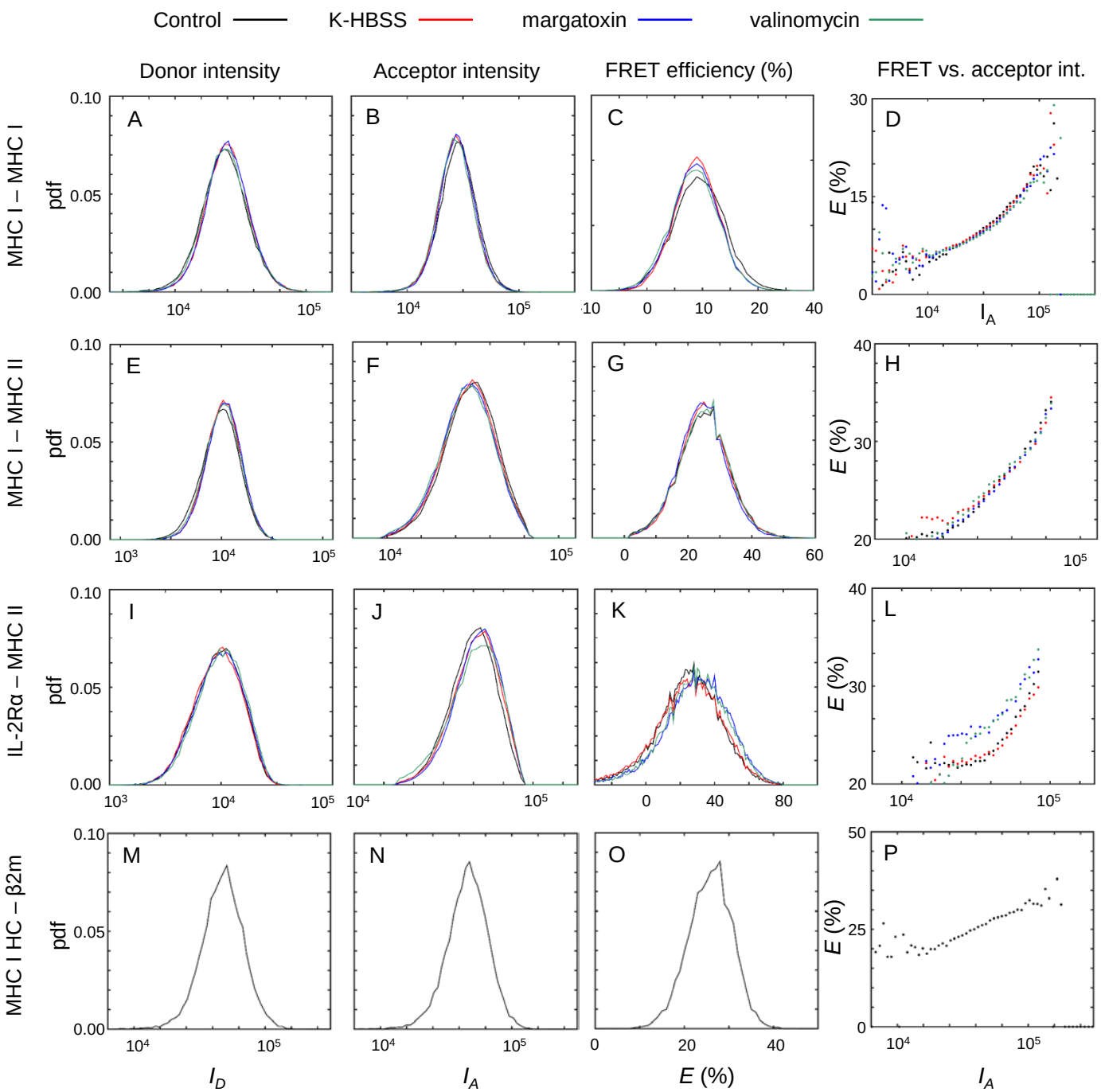

Figure S1

Homo- and heteroassociations of membrane proteins detected by flow cytometric FRET measurements on FT7.10 cells. Proteins were labeled with donor- (Alexa 546) and acceptor-tagged (Alexa 647) mAbs. The top row (panels A-D) displays the homoassociation of MHC I (labeled with A546-W6/32 and A647-W6/32 mAbs). A) Cell-by-cell intensity distributions I_D of donor-tagged MHC I (corrected for FRET quenching); B) Intensity distribution I_A of acceptor-tagged proteins; C) Cell-by-cell average FRET efficiency histograms; D) Dependence of the FRET efficiency E on the acceptor intensity I_A; here, E values were binned within short intervals of I_A. The second and third rows (E-H, I-L) show data for the heteroassociation of MHC I with MHC II (labeled with A546-W6/32 + A647-L243) and of IL-2Rα with MHC II (labeled with A546-anti-Tac + A647-L243) in a similar fashion. The fourth row (M-P) displays FRET measured between the heavy and light chains of MHC I (labeled with A546-W6/32 + A647-L368). This is a mixture of intra- and intermolecular FRET processes occurring between the two chains within the same complex or between chains of distinct, homoassociated MHC I complexes; hence the increase of E upon increasing acceptor intensity (and total MHC I expression). Control samples were incubated in HBSS, depolarization was achieved either by K-HBSS buffer or by margatoxin; hyperpolarization was induced by valinomycin. N~55000, 75000, 55000 and 17000 cells were measured for the different D-A pairs.

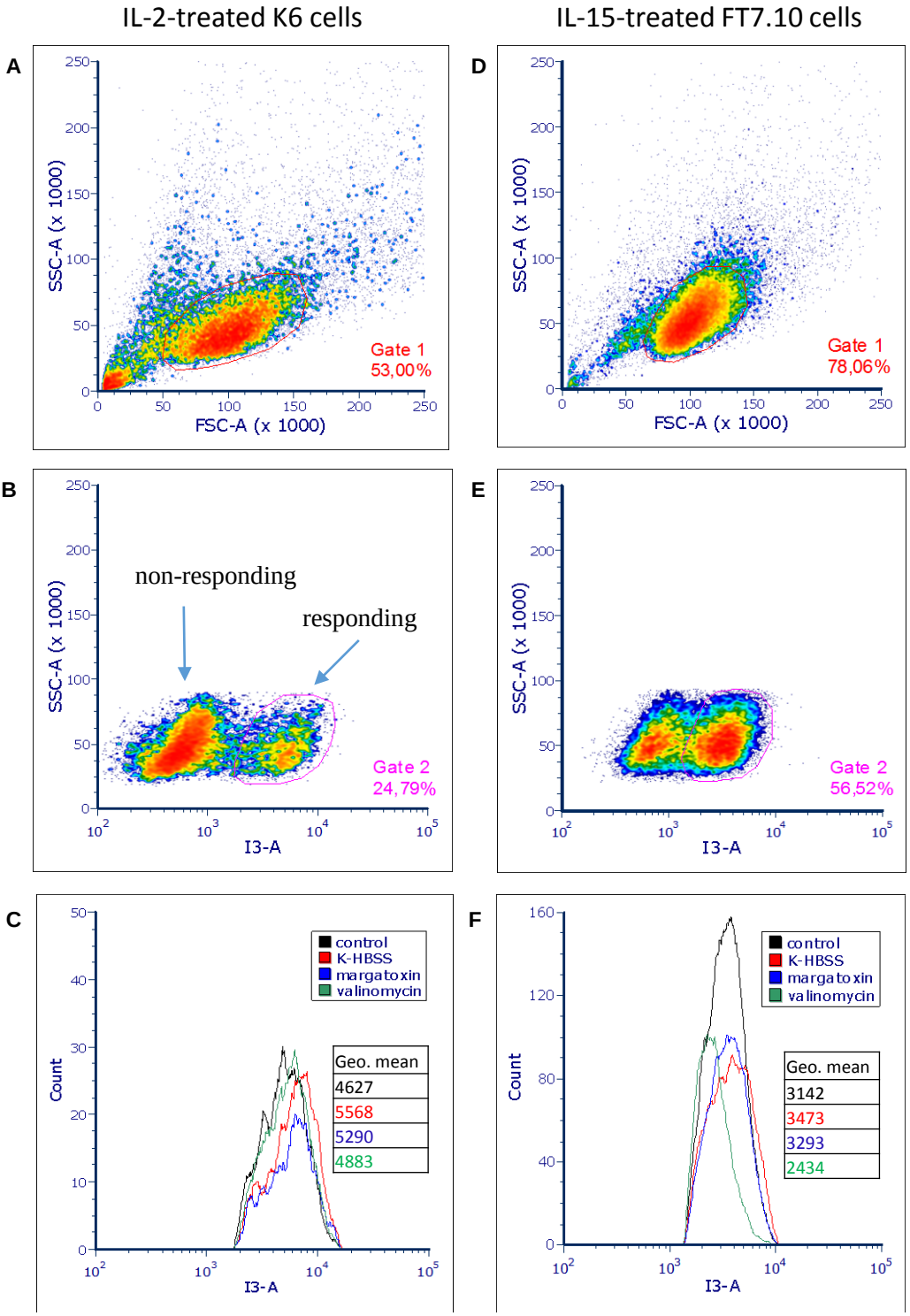

Figure S2

Flow cytometric analysis of IL-2/IL-15 induced STAT5 phosphorylation. Flow cytometry was used to measure STAT5 phosphorylation on a cell-by-cell basis using Alexa647-anti-PSTAT mAbs. Control samples were incubated in HBSS, depolarization was achieved either by K-HBSS buffer or by margatoxin (1.5 nM); hyperpolarization was induced by valinomycin (10 µM). A-C) K6 cells were stimulated with IL-2 (50 pM, 10 min, 37°C). D-F) FT7.10 cells were treated with IL-15 (50 pM, 5 min, 37°C). First, debris was excluded on the side scatter vs. forward scatter plot (panels A, D showing data of the control sample). Next, populations responding to the IL-2/IL-15 treatment were selected on a SSC vs. I3 (PSTAT5) plot (panels B, E showing the control sample); this plot allowed a better separation between responding and non-responding populations than the I3 histograms. Panels C and F display the I3 intensity histograms of the PSTAT5 signals of control, depolarized and hyperpolarized samples. Geometric means of I3 are also shown for the presented experiments.

Charge distribution in and near the transmembrane regions of IL-2/IL-15 receptor subunits, MHC glycoproteins and the transferrin receptor

The electric field across the plasma membrane can act on proteins having an uneven charge distribution in or near their transmembrane regions (TMRs). We identified TMRs of membrane receptors by using an online transmembrane protein topology prediction program (1) or the UniProt database. All four receptor subunits of IL-2/15R have single transmembrane helices. The TMR (bold letters) and 10 flanking amino acids for these proteins are shown below; negatively charged amino acids are marked red and are singly underlined, positively charged ones are blue and doubly underlined. Also shown are examples of one allele each of MHC I and II chains: the HLA-A-68 allele and HLA-DR A α chain, and the transferrin receptor.

IL-2Rα: 231-ETSIFTTEYQ**VAVAGCVFLLISVLLLSGLTW**QRRQRKSRRTI

IL-15Rα: 196-VYPQGHSDTT**VAISTSTVLLCGLSAVSLLACYL**KSRQTPPLAS

IL-2/15Rβ: 233-PAALGKDTIP**WLGHLLVGLSGAFGFIILVYLL**INCRNTGPWL

γ_c: 253-ENPFLFALEA**VVISVGSMGLIISLLCVYFWL**EQTMPRIPTL

HLA-A-68: 296-LRWEPSSQPT**IPIVGIIAGLVLFGAVITGAVVAAV**MWRRKSSDRK

HLA-DR-A α chain: 209-SPLPETTENV**VCALGLTVGLVGIIIGTIFII**KGVRKSNAAE

Transferrin receptor: 58-KPKRCSGSIC**YGTIAVIVFFLIGFMIGYLGY**CKGVEPKTECE

IL-2Rα contains two negatively charged glutamic acids (E-231, E-238) near the extracellular side of the TMR and six positively charged amino acids, five arginines (R) and a lysine (K) near the intracellular side of the TMR. The dipole moment points inward, toward the intracellular side. IL-15Rα contains a potentially positively charged histidine (H-201) and a negatively charged aspartate (D-203) near the extracellular side of the TMR, and two positively charged amino acids near the intracellular side of the TMR (K-229, R-231). Histidine has a pK of 6.0, so H-201 may be positive at physiological pH. The dipole moment may point inward, but it is probably smaller than that of IL-2Rα because there are fewer positive charges near the intracellular side of the TMR and because H-201 may partially cancels the effect of D-203 at the extracellular side. The shared β chain of IL-2R and IL-15R contains a positive and a negative charge (K-233, D-234) next near to each other near the ec. side of the TMR, and a positive charge (R-268) near the intracellular side of the TMR; it also possesses a histidine inside the TMR. The shared γ_c chain has two negative charges (E-253, E-261) near the ec. side, and a negative (E-284) and a positive (R-289) charge near the ic. side of the TMR. The MHC I allele shown has a positively and a negatively charged amino acid in the vicinity of the ec. side and five positive residues near the ec. side of the TMR. HLA-DR A α chain has two negatively charged residues (E-2013, E-216) near the ec. side of the TMR, and three positively charged residues and a negative one at the ic. side. The transferrin receptor differs from the other studied

proteins in that it has three positive charges at the extracellular flank of the TMR; it also has two positive charges at the cytoplasmic flank. From the studied proteins IL-2Rα and HLA-A-68 stand out with their largest positive net charges near the ic. side of the TMR (6 and 5 positive amino acids, respectively).

Supporting reference

1. Kahsay, R. Y., G. Gao, and L. Liao. 2005. An improved hidden Markov model for transmembrane protein detection and topology prediction and its applications to complete genomes. Bioinformatics 21:1853-1858.